



# MICROPHONE ARRAYS IN A WIND TUNNEL ENVIRONMENT WITH A REVERBERATING FLOOR

Marie Pelz<sup>1</sup>, Dirk Döbler<sup>2</sup>, and Jörg Ocker<sup>3</sup>

<sup>1</sup>Technical University of Berlin

Straße des 17. Juni 135, 10623 Berlin, Germany

<sup>2</sup>GFaI e.V.

<sup>3</sup>Porsche AG

## Abstract

The usage of a microphone array is determined for freefield conditions in most cases, which does not hold for measurements in a wind tunnel. Whereas the walls can be assumed as sound-absorbing, this is not correct for the floor. Due to high aerodynamic requirements the floor in a wind tunnel is often a very flat surface which reflects the sound field. For freefield arrays this reflection is leading to a loss of quality. To overcome this degradation, there is the theoretical approach of mirror-ground beamforming using virtual microphones. In the present paper the performance of arrays optimized for freefield conditions is compared with arrays optimized for mirror-ground conditions, which means the application of virtual microphones. By simulations it can be shown that using virtual microphones either leads to a gain of information or enables the reduction of the real microphones' number. In contrast, wind tunnel measurements suggest a drastic loss of coherence between the signals of source and reflection due to turbulent effects. Therefore, the advantages of mirror-ground beamforming are relativised.

## 1 INTRODUCTION

Experimental set-ups in a wind tunnel are often examined with a so called microphone array, usually being a twodimensional arrangement of microphones. Typically, such an array is designed to be used under freefield conditions, which means a room without any boundaries. For a wind tunnel this assumption is not true: Whereas its walls can be assumed as sound-absorbing, in most cases the floor is a very flat surface due to high aerodynamic requirements. Consequently, the freefield becomes a half-space and the sound is reflected at the floor.

The present paper investigates if this sound reflection can be integrated in the beamforming process yielding to a gain of information. If this intent was successful, in addition to the retrieval

of information, the economic effect would be remarkable. An appropriate procedure could enable reducing the number of the array's microphones.

For that purpose, the performances of arrays optimised for the use under freefield conditions are compared to arrays optimised for mirror-ground beamforming by simulations. Therefore, the theoretical background of mirror-ground beamforming is outlined in the beginning. Afterwards, the results of the mentioned simulations are presented. In the end, real wind tunnel measurements are evaluated to estimate the practical relevance of mirror-ground beamforming.

Detailed information about the herein presented results can be found in [6].

## 2 THEORY

The following sections outline the theoretical background of the method of mirror-ground beamforming and the optimisation algorithm which is used to generate the microphone arrays compared in this paper.

### 2.1 Mirror-Ground Beamforming

As the reflection of a sound source is at least partly coherent to its origin, standard beamforming methods fail [3]. One approach to overcome this limitation is the method of mirror-ground beamforming. A reverberating floor is modeled by a freefield in which each source  $S$  is extended by a mirror source  $S'$ . The sound field arising by this is symmetric to the reflecting floor and can be „measured“ by a virtual array. Such an array is generated by reflecting the coordinates of the real microphones at the floor and filling them with virtual microphones. Thus, the overall number of microphones is doubled while the number of real microphones remains constant. The virtual microphones then receive the mirrored sound signal. The described procedure is displayed exemplarily in Fig. 1.

One method to implement virtual microphones mathematically is the extension of the steering vector and the cross spectral matrix, as revealed by CHRISTENSEN and HALD in [2]. The first step is to define steering vectors for the real and virtual microphones:

$$\begin{aligned} g &= [g_m] \text{ and } h = [|g_m|^2] \\ \hat{g} &= [g_j] \text{ and } \hat{h} = [|\hat{g}_j|^2] \end{aligned} \quad (1)$$

Herein,  $m$  indicates the real microphones from 1 to  $M$  and  $j$  from 1 to  $J$  indicates the  $m$ -th mirrored virtual microphone. The extension then leads to:

$$\tilde{g} = \begin{bmatrix} g \\ \hat{g} \end{bmatrix}, \tilde{h} = \begin{bmatrix} h \\ \hat{h} \end{bmatrix} \text{ and } \tilde{C} = \begin{bmatrix} C' & C' \\ C' & C' \end{bmatrix} \quad (2)$$

$C'$  is the cross spectral matrix with diagonal removal. In the last step, an image function  $J$  is derived:

$$J^2(\omega, r) = \frac{1}{\sqrt{2M(2M-2)}} \frac{|\tilde{g}^+ \tilde{C} \tilde{g}|}{\sqrt{\tilde{h}^+ \tilde{\mathbb{I}} \tilde{h}}} \quad (3)$$

Again,  $M$  is the number of microphones.  $\omega$  is the angular frequency,  $r$  the location in which  $J$  is determined and  $\tilde{\mathbb{I}}$  is a  $2M \times 2M$  identity matrix, whose diagonal elements are set to zero. The

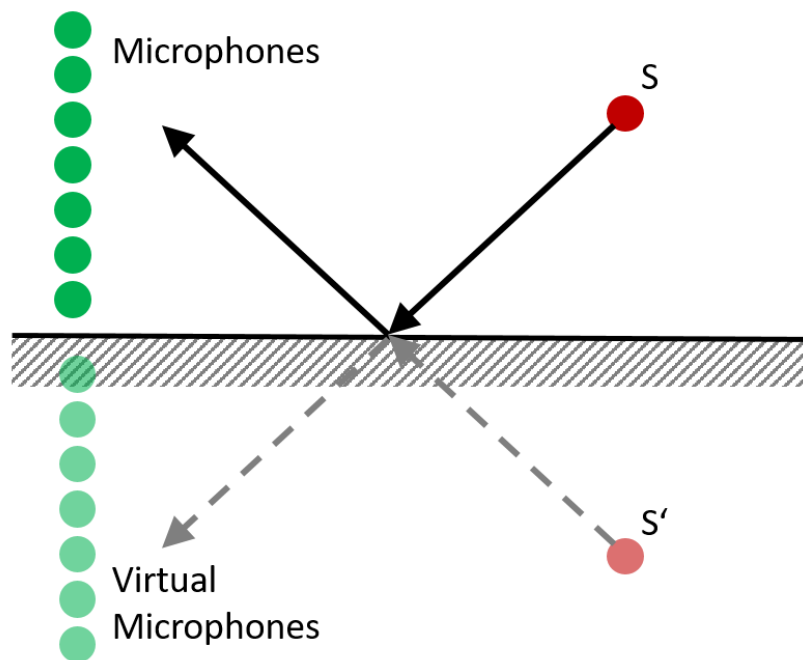


Figure 1: Sound reflected at a floor is modeled by a mirror source. The reflected sound field is then “measured” by virtual microphones.

output of this image function is then plotted in the acoustic photo.

## 2.2 Array Optimisation

Three of the four arrays presented in this paper are optimised with a certain algorithm, which can be used with or without virtual microphones. Starting point of the algorithm is an acoustic scene assembled by at least an image area, a sound source and a microphone array. The algorithm then spreads the microphone coordinates randomly in order to achieve the best acoustic quality. In this case, the best acoustic quality is determined by the user’s choice of dynamic range and mainlobe width for the optimised array. In addition, the microphone arrangement is influenced by two more parameters being weighting factors to define an area of interest inside the array if needed. The arrays presented in this paper do not contain an area of interest, therefore the microphone distribution only depends on the desired dynamic range and mainlobe width.

## 3 IMPACT OF A REVERBERATING FLOOR ON THE PERFORMANCE OF A MICROPHONE ARRAY

As stated in the introductory section, in most cases a microphone array is determined for the use under freefield conditions meaning a room without any boundaries. Usually, this requirement is not fulfilled in a wind tunnel thus leading to sound reflections. In this paper, only the sound reflection at the floor is considered.

When trying to evaluate the impact of a wind tunnel’s reverberating floor on the performance

of a microphone array, there are drawbacks that need to be kept in mind – especially when it comes to the interaction between sound and wind what is the usual case in a wind tunnel:

1. The sound source is imperfect meaning an unknown directional characteristic.
2. Also, the floor is imperfect causing absorption, scattering and wavelength dependencies.
3. The sound reflected at the ground needs to pass the boundary layer twice leading to a loss of coherence to its original source.
4. Original and reflected sound are crossing the shear layer at different points, also leading to a loss of coherence.
5. In addition, the distance the reflected sound needs to cover is longer than for the direct sound leading to a smaller sound pressure level.
6. There is frequency-dependent extinction at the microphones if the reflected sounds is phase-shifted by  $180^\circ$  to the direct sound.

In order to overcome this limitations and to estimate the impact of an reverberating floor under perfect conditions, various simulations were set up. The parameters utilised for the simulations can be gathered from Table 1. Herein, the sound source is a monopole and the reflection is supposed to be perfectly specular. Moreover, the decrease of the sound pressure level due to the longer distance of the reflected sound and the frequency dependent extinction is taken into account in the simulation.

*Table 1: General simulation parameters.*

<b>Parameter</b>	<b>Value</b>
Source	Monopole with White Noise, 80 dB RMS
Third-Octave Bands	100 Hz to 10 kHz
Location of Sound Source	(-0,33 m; -0,165 m; -4,18 m)
Image Area	5 m $\times$ 3 m
Samplingrate	48 kS/s
Simulation Duration	5 s
Resolution	1 pixel $\hat{=}$ 1 cm <sup>2</sup>

For the mentioned simulations three arrays have been generated using the algorithm described in section 2.2. The parameters employed for the optimisation are given in Table 2. Values for dynamic range and mainlobe width cannot be specified as they are adapted simultaneously to the optimisation.  $\lambda_i$  being equal to 1 means that there is the same weighting between the different areas in the optimisation algorithm mentioned in the section above. Therefore, the microphone distribution is only influenced by the required dynamic range and mainlobe width.

Table 2: Parameters used for optimisation.

Parameter	Value
Optimised Frequency	5000 Hz
Size of Array	5 m × 2,5 m (symmetry)
Weighting Factors	$\lambda_1 = \lambda_2 = \lambda_3 = 1$

All the evaluated arrays have been simulated under three conditions: freefield, mirror-ground and mirror-array condition. The mirror-ground condition is a freefield extended by a reverberating floor. Applying the mirror-array condition means adding the virtual microphones to the mirror-ground condition. The acoustic maps arised in these ways were used to assess the array's dynamic range and mainlobe width for every third-octave band in the range given in Table 1.

### 3.1 Freefield Array without Optimisation for Mirror-Ground Beamforming

This array holds 192 microphones whose arrangement was optimised for the use under freefield conditions, its geometry is displayed in Fig. 2. Figure 3 shows the microphone distribution with the use of virtual microphones as applied for mirror-array conditions. The comparison of dynamic range and mainlobe width for freefield, mirror-ground and mirror-array conditions is depicted in Fig. 4, 5 and 6. The acoustic maps for all the three conditions for the third-octave band of 5000 Hz are illustrated in Fig. 7. All of the following acoustic maps are displayed with a dynamic range of 20 dB.

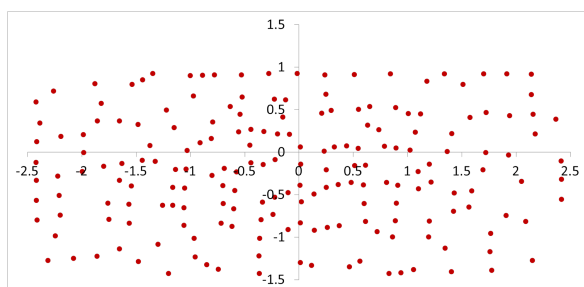


Figure 2: Geometry of the 192 channel array without optimisation for virtual microphones.

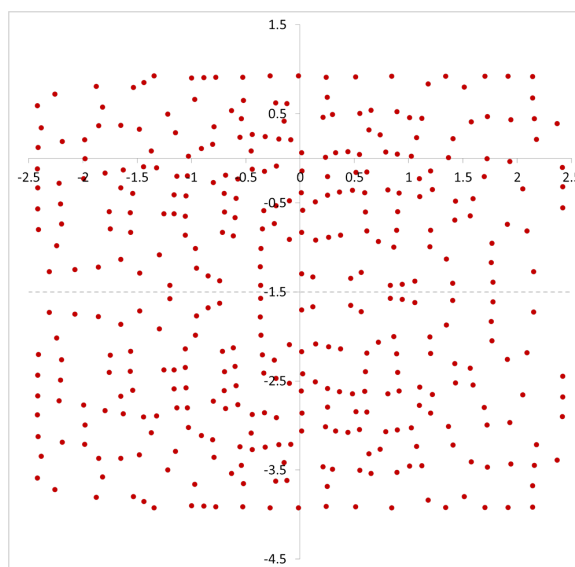


Figure 3: Geometry of the 192 channel array without optimisation for virtual microphones, but with virtual microphones.

The comparison of the dynamic range under the three considered conditions shows that the

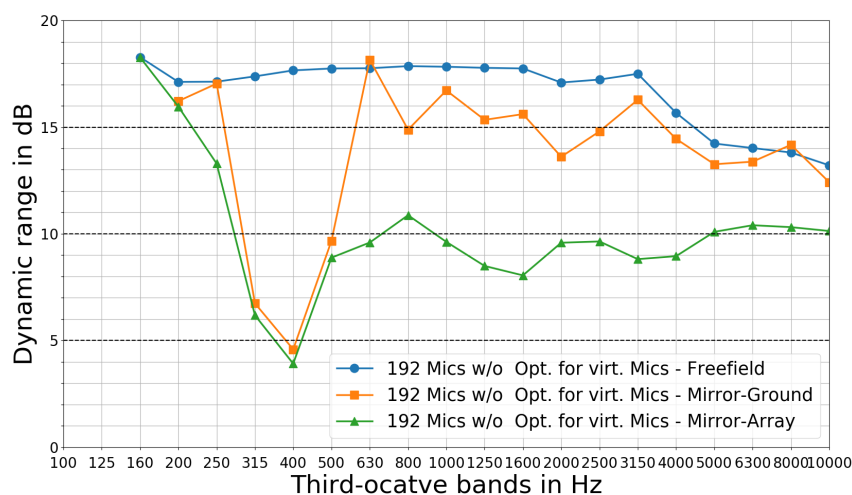
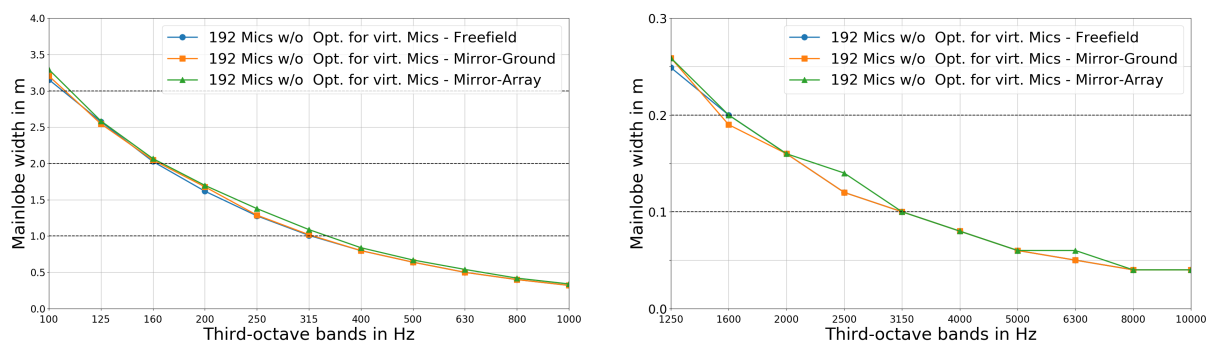


Figure 4: Dynamic range of the 192 channel array without optimisation for virtual microphones.



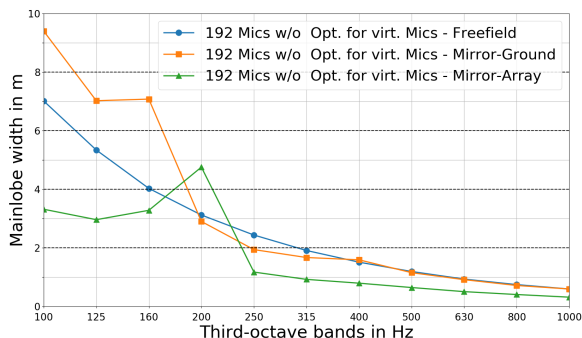
(a) Mainlobe width for the third-octave bands from 100 to 1000 Hz

(b) Mainlobe width for the third-octave bands from 1250 to 10 kHz

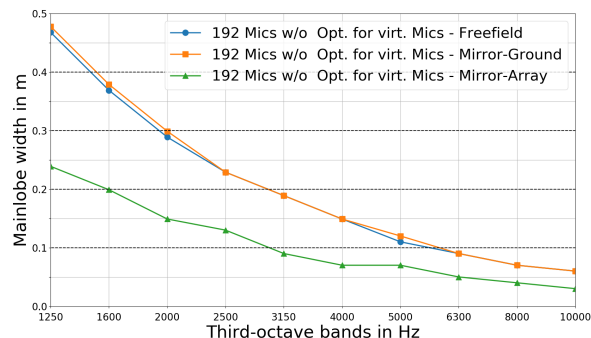
Figure 5: Mainlobe width of the 192 channel array without optimisation for virtual microphones in  $x$ -direction.

array's performance is strongest under freefield conditions and weakest under mirror-array conditions. With respect to [7], this was anticipated as the array's geometry was not optimised for the usage of virtual microphones. Therefore, as depicted in Fig. 7c, strong sidelobes near the mainlobe appear, leading to a decreased contrast. In addition, when examining mirror-ground conditions, the sidelobes of the reflection's PSF interfere with the source's PSF. Hence, the dynamic range is diminished in this case. Also, there is a striking drop in the dynamic range for the third-octave bands of 315, 400 and 500 Hz for the mirror-ground and mirror-array conditions. Here, the sidelobes of the reflection enter the image area very early.

Whereas the mainlobe width in  $x$ -direction is hardly influenced by the different conditions, the mainlobe width in  $y$ -direction is clearly the smallest under mirror-array conditions due to the array's bigger dimension in this direction. The increased mainlobe width for low frequencies is



(a) Mainlobe width for the third-octave bands from 100 to 1000 Hz



(b) Mainlobe width for the third-octave bands from 1250 to 10 kHz

Figure 6: Mainlobe width of the 192 channel array without optimisation for virtual microphones in  $y$ -direction.

caused by the rayleigh criterion. This holds true for all the following arrays when the reflection is taken into account.

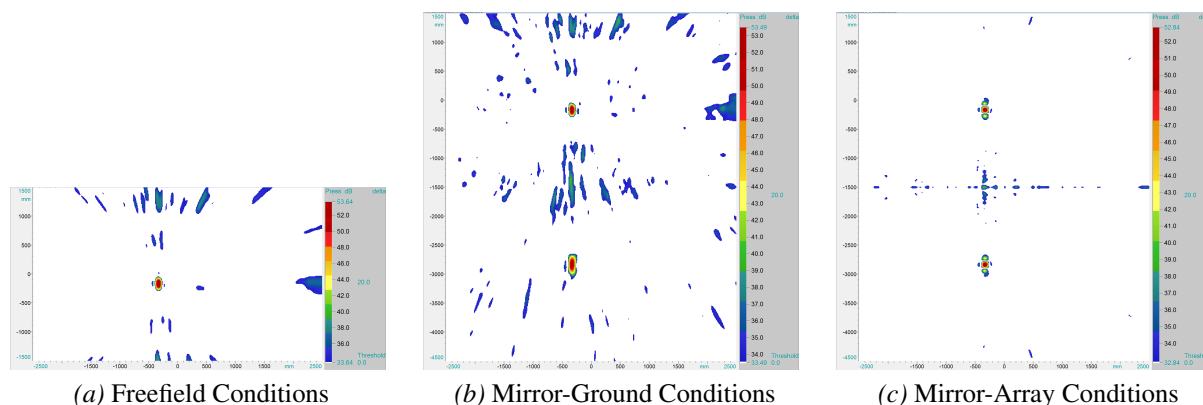


Figure 7: Acoustic maps for the 5000 Hz third-octave band and a contrast of 20 dB, measured with the 192 channel array without optimisation for virtual microphones.

The acoustic maps in Fig. 7 underline the described effects. The map under mirror-ground conditions in Fig. 7b shows a higher sidelobe level than the map under freefield conditions. In contrast, the map under mirror-array conditions is much cleaner which means an overall lower level of sidelobes. At the same time, the sidelobes near the mainlobe show a high sound pressure level yielding to the decreased contrast for mirror-array conditions.

### 3.2 Array with Optimisation for Mirror-Ground Beamforming and 96 Microphones

This array includes 96 real microphones and was optimised for the application of virtual microphones. Thus, the density of microphones is slightly higher in the lower part of the array being the part closer to the ground, as depicted in Fig. 8. The microphone coordinates with

the application of virtual microphones are displayed in Fig. 9. This underlines the prescribed effect of a higher microphone density near the ground which is now the centre of the overall array. Also, this fact is contrary to the geometry of the above shown freefield array having a quite smooth microphone distribution over the whole array's area.

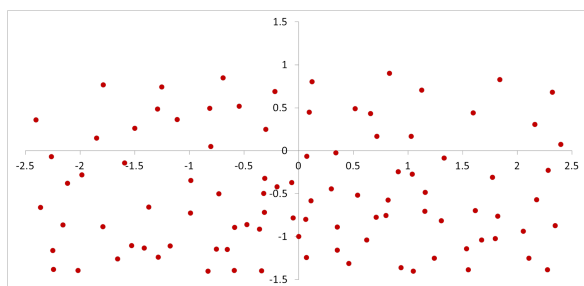


Figure 8: Geometry of the 96 channel array with optimisation for virtual microphones.

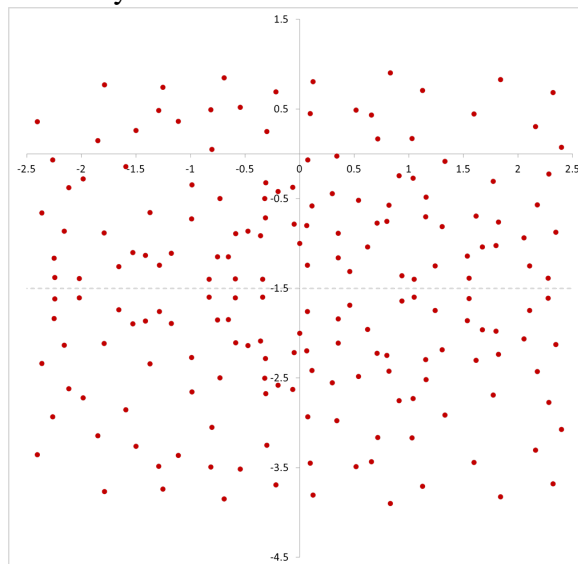


Figure 9: Geometry of the 96 channel array with optimisation for virtual microphones, displayed with these.

The 96 channel-array being optimised for virtual microphones leads to the dynamic range displayed in Fig. 10. In this case, the performance under mirror-array conditions is the best one as the dynamic range reaches the highest values as well as the mainlobe width in y-direction is the smallest, see Fig. 12. Again, the differences for mainlobe width in x-direction are insignificant for all the three conditions, as visible in Fig. 11.

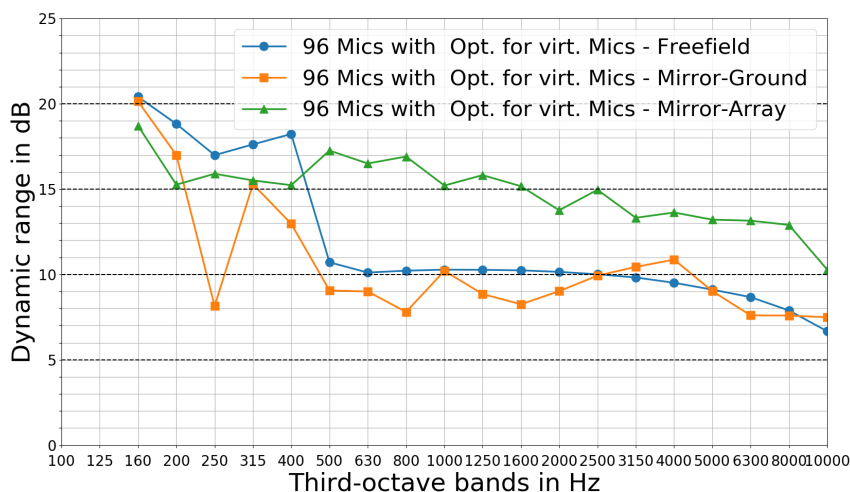
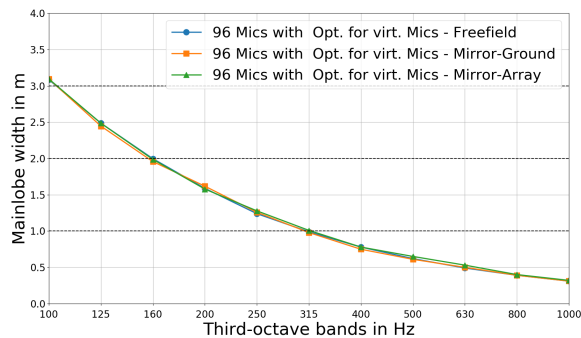
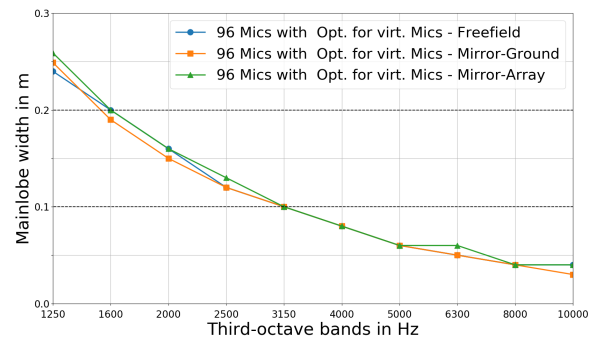


Figure 10: Dynamic range of the 96 channel array with optimisation for virtual microphones.

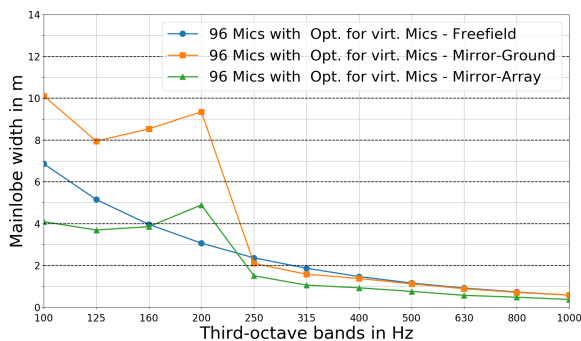


(a) Mainlobe width for the third-octave bands from 100 to 1000 Hz

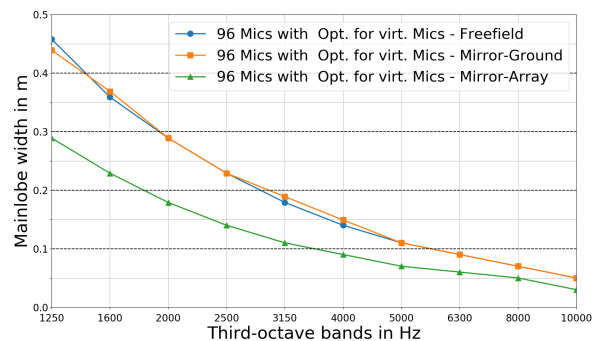


(b) Mainlobe width for the third-octave bands from 1250 to 10 kHz

Figure 11: Mainlobe width of the 96 channel array with optimisation for virtual microphones in  $x$ -direction.



(a) Mainlobe width for the third-octave bands from 100 to 1000 Hz



(b) Mainlobe width for the third-octave bands from 1250 to 10 kHz

Figure 12: Mainlobe width of the 96 channel array with optimisation for virtual microphones in  $y$ -direction.

These observations are emphasised by the acoustic maps illustrated in Fig. 13. For this array optimised for mirror-array conditions the above mentioned strong sidelobes near the mainlobe appear under freefield and mirror-ground conditions. This fact induces the decreased dynamic range for frequencies for 500 Hz and above. In addition, the map for mirror-array conditions is the cleanest of all three maps.

In the same manner an array with 192 real microphones has been generated and investigated. The general effects for this array are similar to those shown above, whereas the bigger array benefits from the higher number of microphones lead to an increased acoustic quality. Further information can be found in [6].

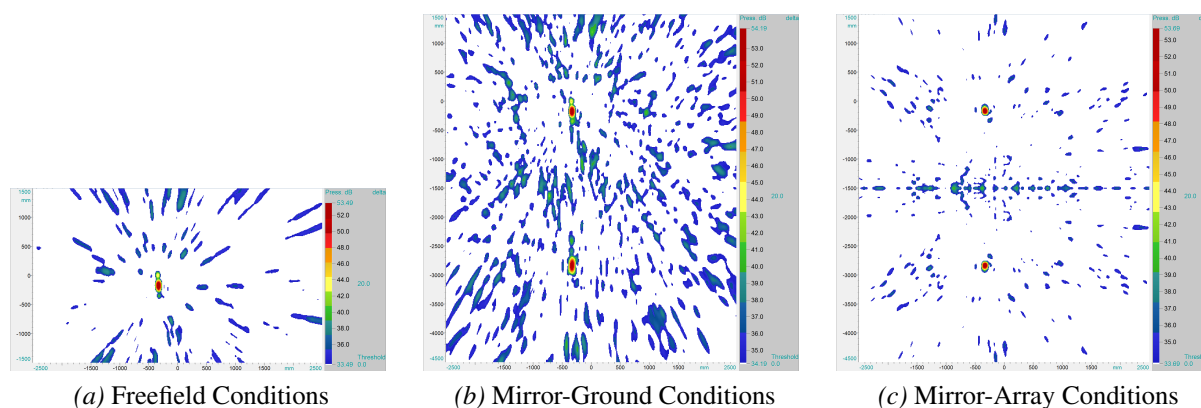


Figure 13: Acoustic maps for the 5000 Hz third-octave band and a contrast of 20 dB, measured with the 96 channel array with optimisation for virtual microphones.

### 3.3 Comparison of Optimised Arrays

In the following, the three optimised arrays (including the array with 192 microphones optimised for virtual microphones which was not shown separately) are compared in the presence of a reverberating floor being simulated by mirror-ground conditions to evaluate their performances in a wind tunnel environment. Therefore, the freefield array is used under mirror-ground conditions as the results for this array implicate that the employment of virtual microphones leads to a worse performance. In contrast, both arrays optimised for the application of virtual microphones are used with those, meaning mirror-array conditions.

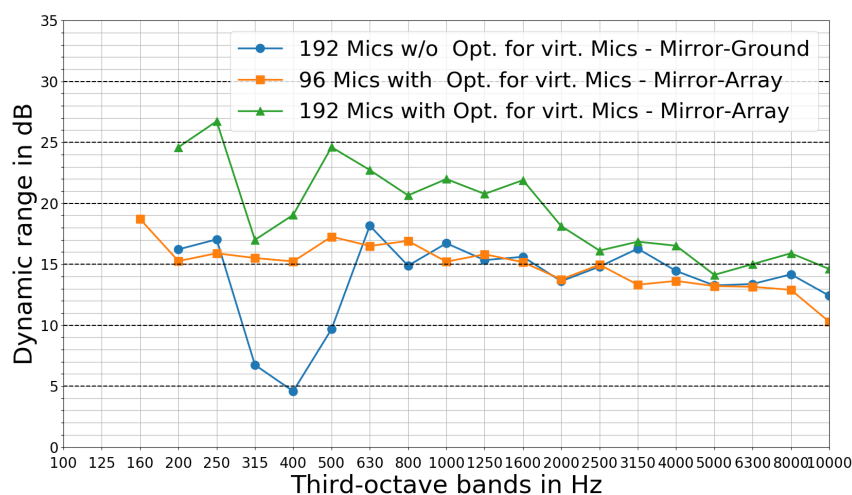
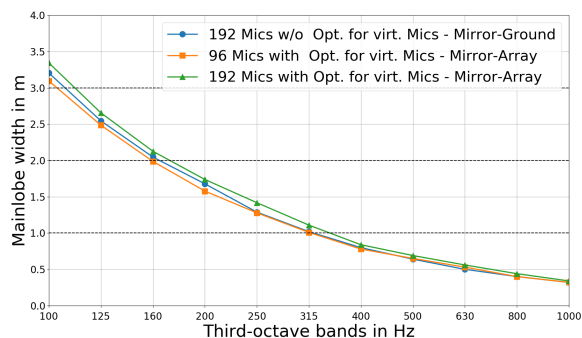
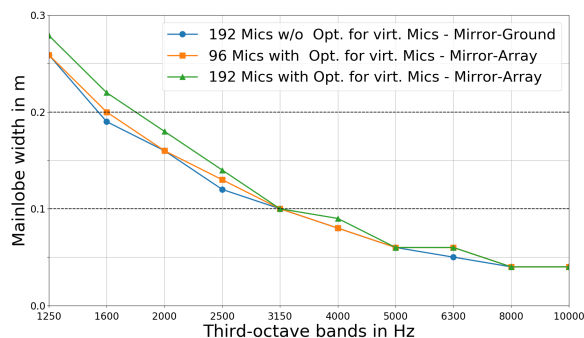


Figure 14: Comparison of the optimised arrays' dynamic ranges.

The dynamic range gathered from the simulations is illustrated in Fig. 14 and shows that the performance of the array optimised for virtual microphones with 192 channels is the best. This was expected as the number of microphones used for the calculation is the highest: with 192 real and 192 virtual microphones there are 384 microphones in the simulation. In addition, under the

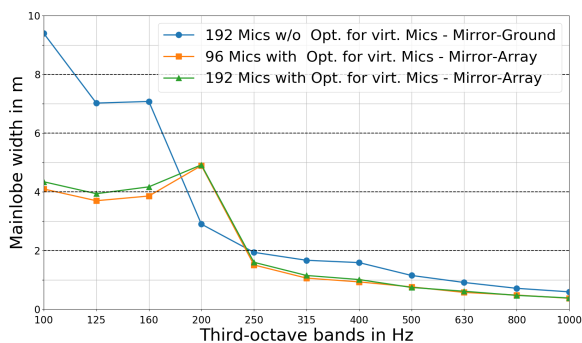


(a) Mainlobe width for the third-octave bands from 100 to 1000 Hz

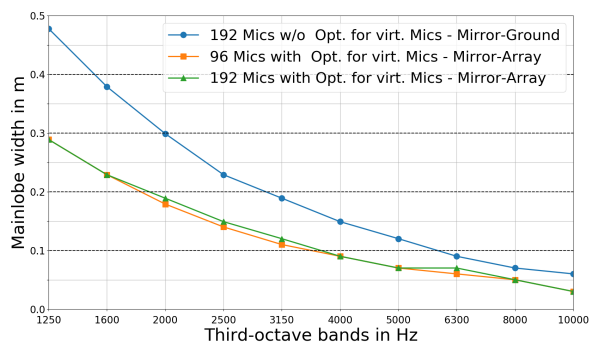


(b) Mainlobe width for the third-octave bands from 1250 to 10 kHz

Figure 15: Comparison of the optimised arrays' mainlobe width in x-direction.



(a) Mainlobe width for the third-octave bands from 100 to 1000 Hz



(b) Mainlobe width for the third-octave bands from 1250 to 10 kHz

Figure 16: Comparison of the optimised arrays' mainlobe width in y-direction.

perfect conditions of a simulation the array with 96 microphones optimised for mirror-ground beamforming gives more or less similar values for the dynamic range as the 192 channel array optimised for freefield conditions. Especially for lower frequencies the freefield array performs worse than the array with 96 microphones.

The mainlobe width in x-direction is hardly effected by the different arrays as the arrays' dimensions in this direction are nearly the same, see Fig. 15. In contrast, the mainlobe in y-direction is the smallest for both arrays used with virtual microphones due to their bigger dimensions in that direction, see Fig. 16.

## 4 RELEVANCE OF MIRROR-GROUND BEAMFORMING

For the purpose of estimating the practical relevance of the mirror-ground beamforming method in a wind tunnel environment, data measured in the wind tunnel in Weissach owned by the PORSCHE AG is consulted. The data itself and the array applied to collect it are described in [4]. The array also holds 192 microphones, was optimised for freefield conditions and is called

real wind tunnel array below.

The recordings used for this evaluation were derived from a speaker mounted on the side window of an automobile. Both speaker and automobile were recorded without wind and with the wind velocities of 100, 140 and 200 km h<sup>-1</sup>. However, only the measurements without wind and with the velocity of 100 km h<sup>-1</sup> are utilised for the following assessment. Therefore, the acoustic map arising from the data with wind has been corrected using the method revealed by AMIET in [1]. The shear layer distance is set up to 1,4 m, the widening angle to 9°. That way, the considered measurements contain all the real influences mentioned in section 3.

#### 4.1 Measurement without Wind

This data is represented by the mirror-ground simulation but with the addition of a real source with an unknown directional characteristic and imperfect reflection. As the sound does not interact with any phenomenons caused by wind this measurement acts as reference.

The acoustic map for this set up is depicted in Fig. 17 and shows no conspicuities. Similarly to the simulation, the reflection appears in the lower part of the picture.

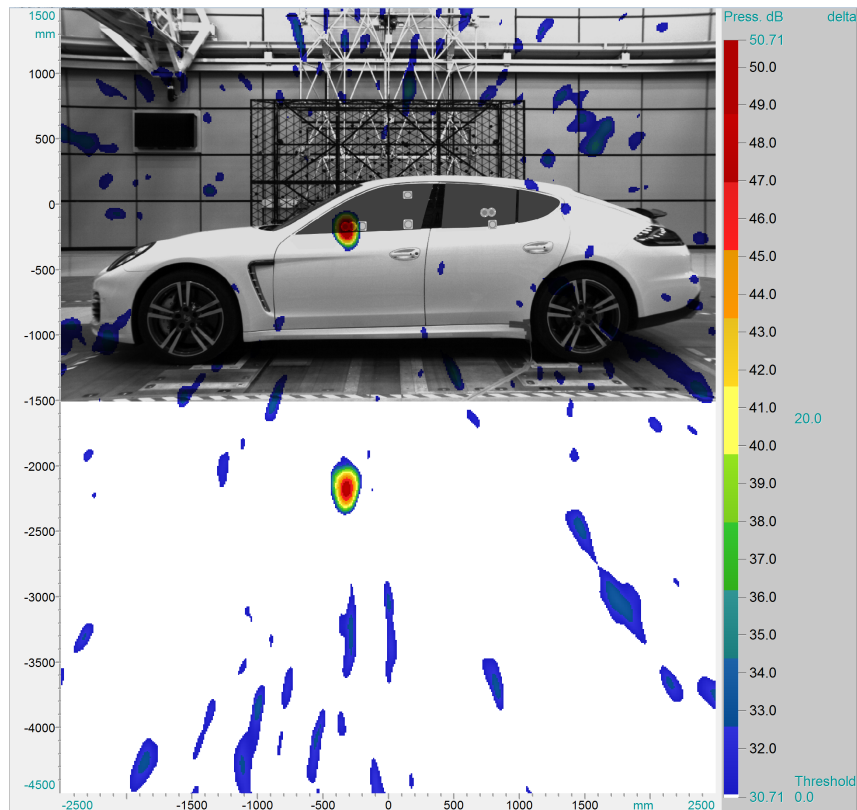


Figure 17: Acoustic maps for the 5000 Hz third-octave band, measured with the real wind tunnel array without wind.

As given in [5] by OERLEMANS, the spectra of source and reflection were derived from the acoustic photo. Those are illustrated in Fig. 18. In addition, the difference between both spectra is displayed. Herein, a positive deviation means that the source is louder than the reflection

which holds true for the predominant part of the frequency domain. This effect arises from the longer distance from its origin to the microphones the reflected signal has to pass. Frequencies for which the reflection is louder than the original source may be caused by the unknown directional characteristic. Moreover, the difference between source and reflection is smaller than 5 dB.

Figure 19 charts the coherence between the time signals of source and reflection. These were gained in the particular maximum. The frequency domain is displayed starting at 224 Hz being the lower threshold frequency of the 250 Hz third-octave band being the first third-octave band for which source and reflection can be indentified as two separate maxima. Clearly, the coherence between both signals is almost 1 for the considered domain. These observations argue for very high reverberative properties of the wind tunnel's floor.

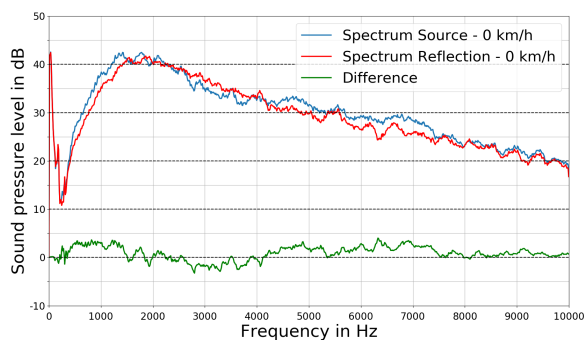


Figure 18: Spectra of measurement with the real wind tunnel array without wind.

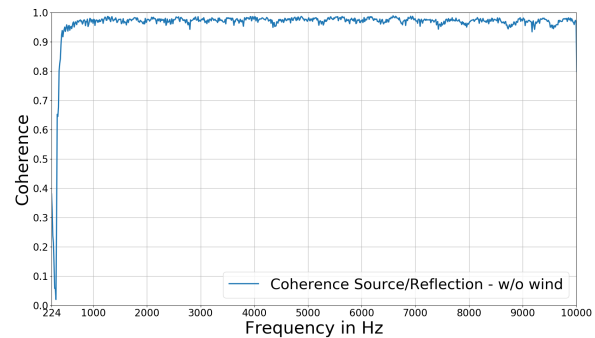


Figure 19: Coherence between source and reflection of the measurement with the real wind tunnel array without wind.

#### 4.2 Measurement with 100 km h<sup>-1</sup> Wind Velocity

In comparison to the measurement described above, at this point data recorded in the presence of wind with a velocity of 100 km h<sup>-1</sup> is evaluated. The corresponding acoustic photo is displayed in Fig. 20. In this case, source and reflection as well as the sidelobes appear less sharp.

Again, the spectra of source and reflection are charted in Fig. 21. It is conspicuous, that the difference between source and reflection is smaller than in the measurement without wind. At the same time, the low frequencies from 0 to appr. 250 Hz seem to be stimulated by wind as the sound pressure level for those is increased.

The coherence shown in Fig. 22 is displayed from 708 Hz on as the 800 Hz third-octave band is the first that allows the separate identification of source and reflection. It can be spotted that the frequency domain in which the signals are coherent being much smaller than for the measurement without wind: from appr. 708 Hz to 5000 Hz. Further, the maximum coherence is decreased compared to the case without wind.

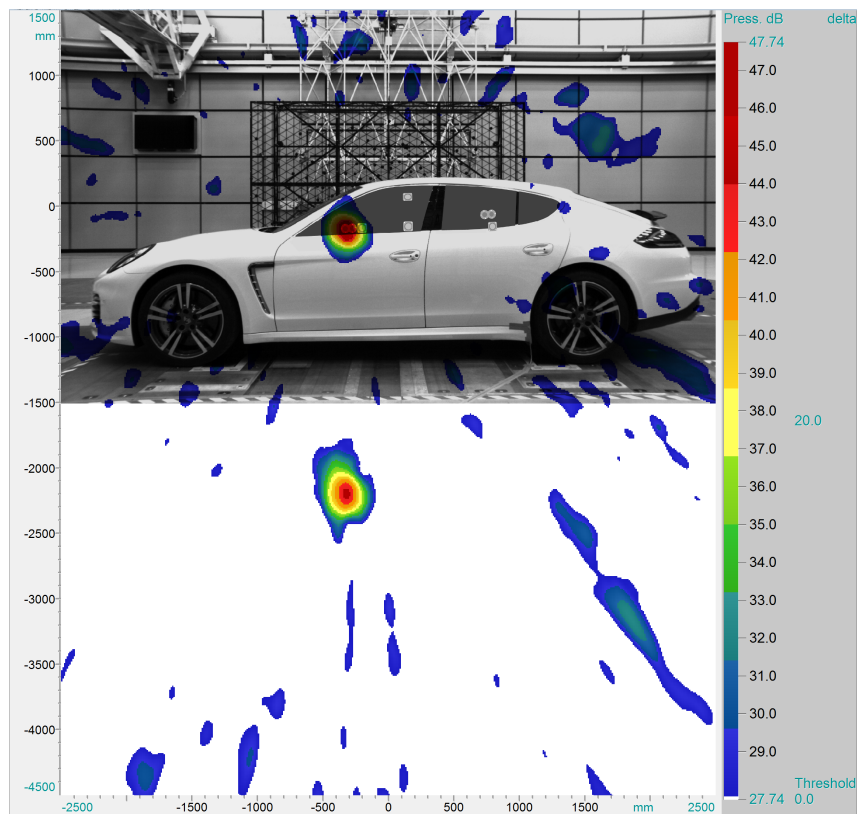


Figure 20: Acoustic maps for the 5000 Hz third-octave band, measured with the real wind tunnel array with  $100 \text{ km h}^{-1}$  wind velocity.

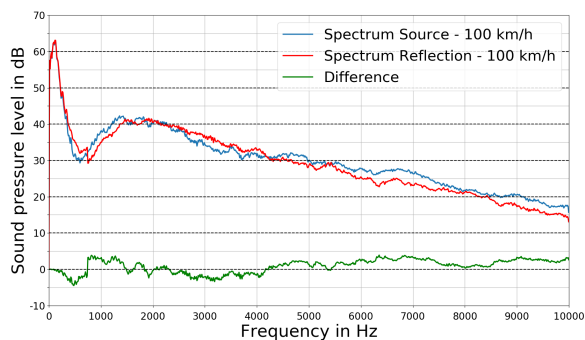


Figure 21: Spectra of measurement with the real wind tunnel array and  $100 \text{ km h}^{-1}$  wind velocity.

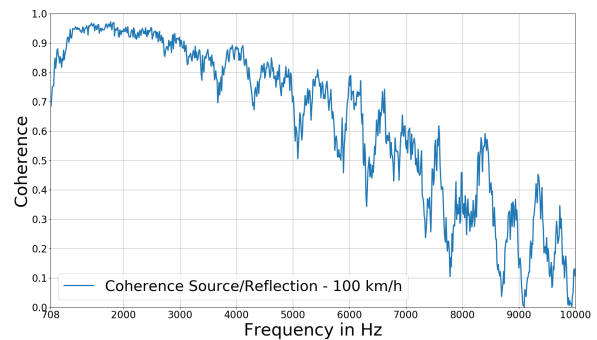


Figure 22: Coherence between source and reflection of the measurement with the real wind tunnel array and  $100 \text{ km h}^{-1}$  wind velocity.

### 4.3 “Simulated” Measurements

The time functions derived from source and reflection for both measurements with and without wind have been used to estimate the performance of the array with 192 microphones optimised

for virtual microphones under the imperfect conditions of a real wind tunnel measurement. Therefore, another simulation with two sound sources was set up: one of the sources was loaded with the real source's time function, the other one with the reflection's time function. In the following figures charting the dynamic range, the 192 channel array with optimisation for virtual microphones is displayed under mirror-array conditions and in comparison to the real wind tunnel array under mirror-ground conditions.

Dynamic range and acoustic map for the case without wind are illustrated in Fig. 23 and 24. Clearly, there are lower values for the optimised array especially for the frequencies up to the 1000 Hz third-octave band. Yet, this array is able to resolve the third-octave bands from 200 Hz to 400 Hz which the real wind tunnel array is not capable of.

For the measurement with  $100 \text{ km h}^{-1}$  wind velocity the dynamic range and acoustic map are depicted in Fig. 25 and 26. Again, the dynamic range of the optimised array is lower than for the real wind tunnel array. Particularly, the drop for the third-octave bands of 300 and 400 Hz is significant. At the same time, the dynamic range for the third-octave band of 1000 Hz is increased strongly. The corresponding measurements suggested a high coherence for the frequencies between 1000 and 3000 Hz being the reason for similar values between the simulation without and with wind. In addition, both acoustic maps are very akin.

Although not all correlations can be fathomed at this point, these simulations affirm the limitations of mirror-ground beamforming which the loss of coherence already indicated.

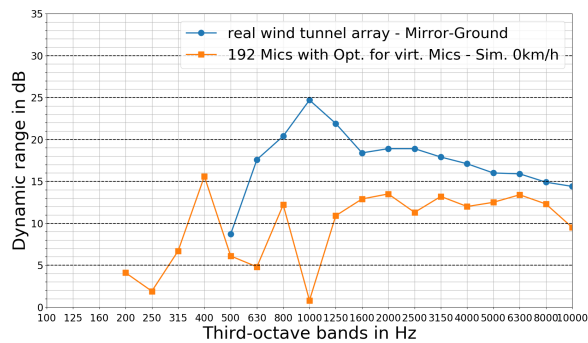


Figure 23: Dynamic range of the 192 channel array with optimisation for virtual microphones without wind.

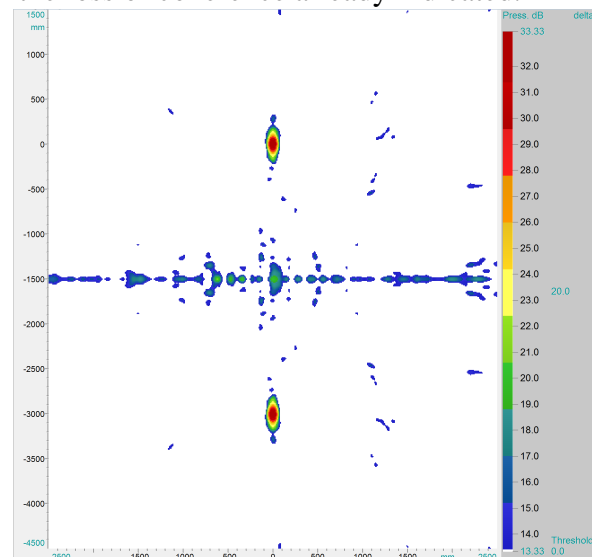


Figure 24: Acoustic map of the 192 channel array with optimisation for virtual microphones without wind for the 5000 Hz third-octave band.

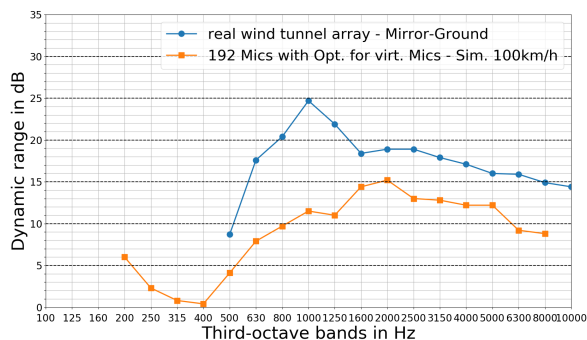


Figure 25: Dynamic range of the 192 channel array with optimisation for virtual microphones and  $100 \text{ km h}^{-1}$  wind velocity.

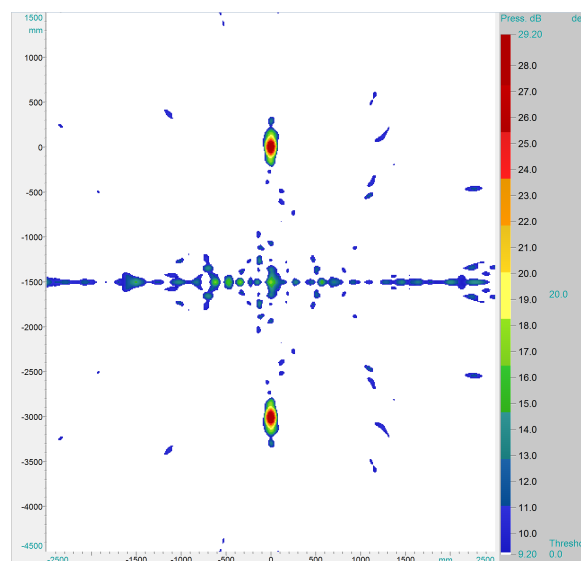


Figure 26: Acoustic map of the 192 channel array with optimisation for virtual microphones and  $100 \text{ km h}^{-1}$  wind velocity for the 5000 Hz third-octave band.

## 5 CONCLUSION

In the present paper microphone arrays were examined and compared referring to their performance in the presence of a reverberating floor. This evaluation aimed at answering the question if the use of virtual microphones is beneficial.

Hence, the simulations in section 3 have shown that under perfect conditions one either gains information leading to an increased dynamic range or that it is possible to reduce the number of real microphones. Especially with respect to economical issues this was profitable. Additionally, due to the enlarged dimensions when using virtual microphones the mainlobe width in the particular direction is diminished also leading to an increase of the spatial resolution. Nevertheless, there is a loss of quality in the corresponding acoustic maps which is the trade-off when reducing the number of microphones leading to a lower microphone density over the array's area.

Furthermore, it has to be stated that a microphone array should operate only under the conditions it is determined for. Freefield arrays should not be utilised with virtual microphones as well as arrays optimised for the application of virtual microphones should only be used with these.

In contrast, the measurements analysed in section 4 implicate that the benefit of virtual microphones is not as high as the simulations suggested. Motivation for the application of mirror-ground beamforming is the coherence between original source and its reflection. Hence, the conditions in the specific wind tunnel in Weissach are close to the simulated mirror-ground conditions as the coherence in this case is nearly one. Therefore, such a test set up might have the potential for a beneficial application of virtual microphones. On the other hand, when it

comes to the interaction of sound and turbulent effects caused by wind the coherence is decreased significantly. This fact challenges the advantages of mirror-ground beamforming for real wind tunnel measurements.

## References

- [1] R. K. Amiet. “Refraction of Sound by a Shear Layer.” *Journal of Sound and Vibration*, 58(4), 467 – 482, 1978.
- [2] J. J. Christensen and J. Hald. “Beamforming.” Technical Review No. 1 - 2004, 2004. Brüel & Kjær Sound & Vibration Measurements A/S.
- [3] S. Guidati, G. Guidati, and S. Wagner. “Beamforming in a reverberating environment with the use of measured steering vectors.” In *AIAA/CEAS Aeroacoustics Conference and Exhibit, Maastricht, Netherlands, May 28-30, 2001*. 2001.
- [4] J. Ocker and S. Tilgner. “The Porsche Wind Tunnel Microphone Array System.” *Aachen Acoustics Colloquium*, pages 135 – 151, 2015.
- [5] S. Oerlemans, L. Broersma, and P. Sijtsma. “Quantification of Airframe Noise Using Microphone Arrays in Open and Closed Wind Tunnels.” *Int. J. Aeroacoustics*, 6(4), 309–333, 2007.
- [6] M. Pelz. “Gegenüberstellung der Leistungsfähigkeit von Mikrofon-Arrays in einer Windkanalumgebung unter Berücksichtigung des schallharten Bodens.”, 2017.
- [7] P. Sijtsma and H. Holthusen. “Corrections for mirror sources in phased array processing techniques.” In *9th AIAA/CEAS Aeroacoustics Conference and Exhibit, Hilton Head, South Carolina, May 12-14, 2003*. 2003. URL <http://www.nlr.nl/smartsite.dws?id=2862>.